IEEE TRANSACTIONS ON

INDUSTRIAL ELECTRONICS

NOVEMBER 2017 VOLUME 64 NUMBER 11 ITIED6 (ISSN 0278-0046)

PAPERS

(Contents Continued on Page 8393)

A PUBLICATION OF THE IEEE INDUSTRIAL ELECTRONICS SOCIETY

Wind Turbine With Mechanical Power Split Transmission to Reduce the Power Electronic Devices: An Experimental Validation

Qian Liu, Rüdiger Appunn, and Kay Hameyer, *Senior Member, IEEE*

***Abstract*—This paper describes the structure, control, and performance of a novel concept wind turbine with a planetary gearbox. The power extracted from the wind is split into two parts by a free-running planetary gearbox. The major part of the power is delivered to a synchronous generator that is directly connected to the power grid without any power electronic devices. Only a very small part of the power is delivered to a servo machine that is controlled by a small-scale back-to-back converter. The servo machine operates the sun gear of the planetary gearbox. In order to show the variable speed operation with maximum power point tracking of the wind turbine at both low and high wind speed, a test bench is constructed and several experiments are performed. The experimental results in both steady state and transient state validate the performance and power split behavior of the wind turbine. The power ratio of the back-to-back converter in the new wind turbine is much smaller than the one in conventional wind turbines, which implies the possibility to reduce the power electronic devices.**

***Index Terms*—Experimental validation, mechanical power split, planetary gearbox, reduction of power electronic devices, wind turbine.**

I. Introduction

NOWADAYS, due to the environmental consideration, the renewable energy especially the wind energy plays an important role in the energy market. Moreover, for the offshore wind turbines, the rated power of a single wind turbine is growing toward 10 MW to improve the utilization of the wind energy. In the wind energy market, the existing wind turbines can be distinguished into two main categories: wind turbines with doubly fed induction generators (WT-DFIGs) and wind turbines with synchronous generators (WT-SGs).

For the WT-DFIG, the stator of the induction generator is directly connected to the power grid while the rotor is supplied by a partial-scale converter. The power through the converter is usually 30% of the rated power of the wind turbine [1]. Although the WT-DFIG is very popular in the wind energy market and in the research field [2]–[4], it has mechanical difficulty for the large-scale wind turbine. A crucial issue for the doubly fed induction generator (DFIG) is its small air gap. At a large load torque, the deformation and oscillation of the rotor are critical for the DFIG [5]. Therefore, to increase the power rating of the wind turbine, more attention must be payed on the design of the DFIG and the transmission shaft. Moreover, the bear ring in the rotor also hinders the performance of the WT-DFIG [1].

The WT-SG has different types such as wind turbine with an electrically excited synchronous generator [6] or permanent magnet synchronous generator (PMSG) [7]. Moreover, the WT-SG can also be direct drive or with a gearbox. However, no matter what type the WT-SG is, a full-scale converter has to be utilized for the variable speed operation as well as the optimum wind power extraction. For the large-scale wind turbines, the full-scale converter leads to a large size, large weight, high cost, and high-cooling burden. The design and production of a large-scale converter is still under development [1]. Moreover, the full-scale converter results in a large grid side filter. In [8], it is pointed out that the full-scale converter causes more system failure in the wind turbine, when compared to the partial-scale converter.

Therefore, both existing conventional wind turbine structures have difficulties and shortages for the large-scale wind turbine. To increase the rated power of the wind turbine, it is expected that the wind turbine is with the synchronous generator (SG) while the scale of the converter can be reduced. In [9], a new wind turbine with a DFIG and an additional PMSG as an exciter is developed to improve the power quality and fault ride through capability. However, this structure still has a DFIG as the main generator and has the same rotor-side control as conventional WT-DFIG for the variable speed operation. Therefore, the power through the converter and the exciter generator is still about 30% of the rated power of the wind turbine. In [10], a wind turbine with power split, which is realized mechanically by a free-running planetary gearbox, is proposed. This wind turbine contains an SG and a servo machine. The SG is directly connected to the power grid while the servo machine is with a partial-scale converter. A theoretical analysis of the wind turbine with a planetary gearbox is shown in [11] for the power

Manuscript received July 25, 2016; revised October 5, 2016; accepted October 10, 2016. Date of publication October 31, 2016; date of current version October 9, 2017. This work was supported by the Ziel-2-Programm NRW 2007–2013 "Regionale Wettbewerbsfähigkeit und Beschäftigung." *(Corresponding author: Qian Liu.)*

The authors are with the Institute of Electrical Machines, Rheinisch-Westfalische Technische Hochschule Aachen, 52062 Aachen, Germany (e-mail: qian.liu@iem.rwth-aachen.de; ruediger.appunn@iem.rwth-aachen.de; kay.hameyer@iem.rwth-aachen.de).

Color versions of one or more of the figures in this paper are available online at http://ieeexplore.ieee.org.

Digital Object Identifier 10.1109/TIE.2016.2622666

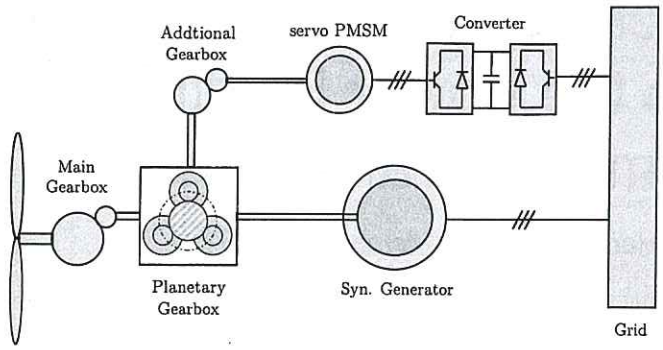

Fig. 1. Structure of the wind turbine with power split.

split behavior. It is pointed out that the power delivered to the partial-scale converter can be less than 10% of the rated power of the wind turbine. In [12], the drive train control is introduced to realize the variable speed operation of a wind turbine with a planetary and a special two-mode gearbox . However, in the aforementioned literature, the feasibility, operation, and power split behavior of the wind turbine with a planetary gearbox lack convincing support such as a test bench and experiments.

This paper is divided into two parts. The first part is the description, analysis, and control of the wind turbine with a special planetary gearbox. Due to the special structure, the drive train control of the wind turbine with power split is carefully designed. In the second part of this paper, a test bench and experimental results for the wind turbine with a planetary gearbox are shown. The experiments are investigated with a constant, ramp, and stochastic wind speed. The variable speed operation with maximum power point tracking (MPPT) and small power ratio to the converter are validated by the experimental results, which show the possibility for the reduction of the power electronic devices.

II. Wind Turbine With Power Split

Similar to the power train of the hybrid electrical vehicles, the structure of the proposed wind turbine with power split is shown in Fig. 1. The main components of the wind turbine with power split consist of a turbine system, a main gearbox, a free-running planetary gearbox, an electrically excited SG, a servo permanent-magnet synchronous machine (PMSM), and a back-to-back converter. The main gearbox is with a one- or two-stage structure so that the rated speed of the main shaft at the high-speed side is about 400–600 r/min. The power split is realized by the planetary gearbox, with which the extracted wind power is delivered to the SG and the servo PMSM. The SG is directly connected to the power grid. Meanwhile, the servo PMSM, which is the main control unit of the drive train, is supplied by a small-scale back-to-back converter. The additional transmission gearbox, which is optional, is used to adjust the speed-torque operating curve of the servo PMSM.

A. Aerodynamics and Power Curve of the Turbine

The turbine system of the wind turbine with power split is the same as that of the traditional wind turbine. The extracted wind power of the turbine system is proportional to the kinetic energy

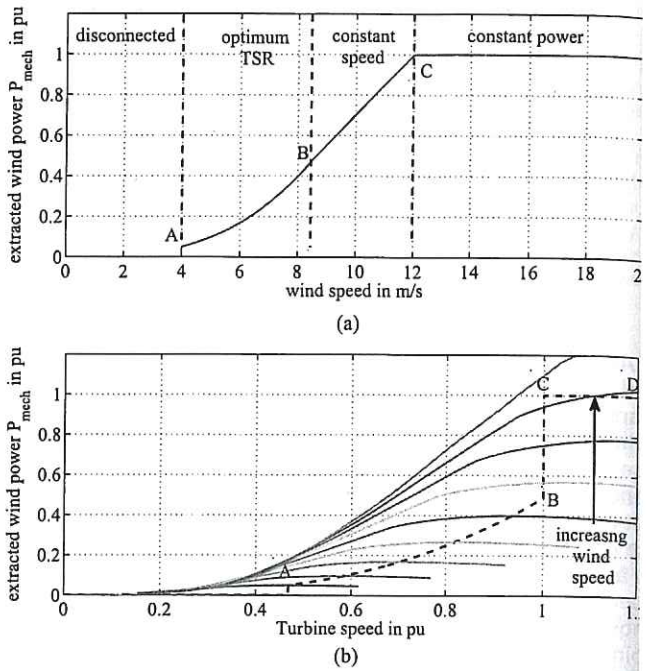

Fig. 2. Power curves of an exemplary wind turbine. (a) Power cur with wind speed. (b) Power curve with turbine speed.

in a cylinder of air traveling with wind speed v_w within the rot swept area of the turbine system [13]. It can be presented by th following equation:

$$P_{\text{mech}} = \frac{1}{2}\rho_{\text{air}}\pi R_t^2 C_p(\lambda,\beta)v_w^3 \quad (1$$

where ρ_{air} is the air density, R_t is the radius of the rotor swe area, $C_p(\lambda,\beta)$ is the performance coefficient, which denotes th percentage of the wind power extracted by the turbine syste $C_p(\lambda,\beta)$ is the function of the tip speed ratio (TSR) $\lambda = \frac{\omega_t R}{v_w}$ and the pitch angle of the blades β, and ω_t is the rotational spee of the turbine. The performance coefficient C_p depends on th structure and aerodynamic characteristics of the turbine. Th maximum value of C_p stays at an optimum pitch angle (usuall at 0°) and an optimum TSR. With the increasing pitch angle, th performance coefficient C_p drops, which reduces the extracte power from the wind.

At low or median wind speed, the turbine system is with th maximum performance coefficient for optimum wind power e traction. At high wind speed, the pitch angle is increased to lim the power and speed of the turbine [14]. Exemplary mechanic power curves of the wind turbine are shown in Fig. 2(a) and b the dashed curve in Fig. 2(b) depending on the wind speed an the turbine speed, respectively. When the wind speed is less tha a given value, which is called the cut-in wind speed, the losse of the wind turbine are larger than the available wind power. Th generator is disconnected from the power grid and the turbin is stalled so that the mechanical power of the turbine become zero. Along the curve between A and B, which is called the op timum TSR region, the pitch angle and the speed of the turbin are controlled to the optimum values so that optimum TSR an the maximum C_p as well as the optimum wind power extractio can be achieved. On the curve between B and C, which is calle

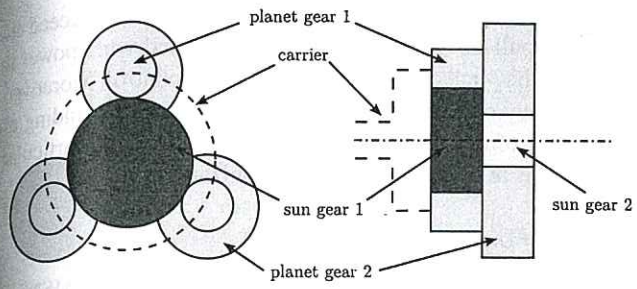

Fig. 3. Structure of the special planetary gearbox.

the constant speed region, the speed of the turbine stays at its rated value and the pitch angle is controlled. The extracted wind power increases with the increment of wind speed until the rated power of the turbine is reached. Due to the limited pitch rate of the wind turbine, it is possible that the turbine speed accelerates above the rated value, which is illustrated by the dashed line between operating points C and D in Fig. 2(b). However, if the pitch rate is large, the overshoot above the rated speed is negligible and the maximum turbine speed can be considered as its rated speed [14]. When the wind speed is higher than a critical value, which is called the cutoff wind speed value, the generator is disconnected from the power grid and the turbine is stalled to protect the wind turbine.

B. Planetary Gearbox

The standard planetary gearbox has three terminals: a ring gear, a sun gear, and a carrier. The structure and dynamic model of the standard planetary gearbox can be found in [15] and [16]. In the proposed wind turbine and the test bench, a special planetary gearbox is utilized to improve the efficiency. The structure of the special planetary gearbox is shown in Fig. 3. When compared to the standard planetary gearbox, the special planetary gearbox has no ring gear. Each planet gear has two different radii, which realize the gear ratio between two sun gears. The two sun gears are separated and actuated by the planet gears that are attached to the carrier.

In the gearbox, the oil friction losses depend on the contact area of the gears [17]. In the special planetary gearbox mentioned above, there is no ring gear with large radius. The contact area in the aforementioned special planetary gearbox is smaller than that in the standard one. Therefore, the oil friction losses can be reduced by the special planetary gearbox [12].

Moreover, sun gear 1, sun gear 2, and the carrier in the special planetary gearbox are equivalent to the carrier, sun gear, and ring gear in the standard planetary gearbox, respectively. The dynamic equation of the special planetary gearbox has the same form as that of the standard one

$$\begin{bmatrix} \dot{\omega}_{s1} \\ \dot{\omega}_{s2} \end{bmatrix} = \begin{bmatrix} -k_{11} & -k_{12} \\ -k_{21} & -k_{22} \end{bmatrix} \begin{bmatrix} \omega_{s1} \\ \omega_{s2} \end{bmatrix} + \begin{bmatrix} a_{11} & a_{12} & a_{13} \\ a_{21} & a_{22} & a_{23} \end{bmatrix} \begin{bmatrix} T_{s1} \\ T_{s2} \\ T_c \end{bmatrix} \tag{2}$$

where T is the torque and the subscripts $s1$, $s2$, and c denote sun gear 1, sun gear 2, and the carrier. The parameters k_{ij} and a_{ij} are the lumped friction and inertia coefficients, respectively. The relationship of the speed is described by the following equation:

$$(1 - i_0)\omega_{s1} = \omega_{s2} - i_0\omega_c. \tag{3}$$

The gear ratio of the plus planetary gearbox i_0 is obtained by the following equation:

$$i_0 = \frac{(r_{p1} - r_{p2})(r_{p2} + r_{s2})}{r_{p1}r_{s2}} \tag{4}$$

where r_{p1}, r_{p2}, and r_{s2} are the radii of planet gear 1, planet gear 2, and sun gear 2, respectively. In the steady state, if the friction is neglected, the model of the special planetary gearbox can be simplified into the following form:

$$T_{s2} = -\frac{1}{1 - i_0}T_{s1} \tag{5}$$

$$T_c = \frac{i_0}{1 - i_0}T_{s1}. \tag{6}$$

Therefore, the special planetary gearbox has the same steady-state model as the standard planetary gearbox shown in [11]. The investigated wind turbine in this paper has the following structure. The main shaft is connected to sun gear 1, the SG is connected to sun gear 2, and the carrier is connected to the additional gearbox that delivers torque to the servo PMSM. The theoretical and practical aspects to scale up the components of a wind turbine such as a gearbox can be found in [18].

C. Minimum Power to Servo PMSM

During the variable speed operation of the wind turbine, the servo machine (PMSM) is operated in both generator and motor mode. For the power delivered to the servo PMSM and the converter, the same analysis for the power split behavior as shown in [11] is supplied. There is no explicit function between the real-time demanded power of the servo PMSM and the turbine power. Since the special planetary gearbox has the same steady-state model as the standard planetary gearbox, all the conclusions for the minimum power split in [11] can be directly applied for the wind turbine structure in Fig. 1. In the analysis, the wind turbine is assumed in ideal operation and the losses in the gearboxes are neglected. The minimum power split depends on the gear ratios of the main and planetary gearboxes. Denoting $P_{\text{servo},N}$ and $P_{t,N}$ as the peak mechanical power of the servo PMSM in the full wind speed range and the rated mechanical power of the turbine, the minimum ratio $b_{\min} = \min\{\frac{|P_{\text{servo},N}|}{P_{t,N}}\}$ can be obtained by $b_{\min} = 1 - a_{\text{opt}}$, where a_{opt} is the solution of the following equation:

$$1 - a_{\text{opt}} = \frac{4}{27}\frac{P_B}{P_{t,N}}a_{\text{opt}}^3. \tag{7}$$

Here, P_B is the mechanical power of the turbine at the end of the optimum TSR region, which is illustrated by the operating point B in Fig. 2. However, to reach the minimum power for the servo PMSM, the gear ratios of the main and planetary gearboxes have to fulfill the following relationship:

$$i_0 = 1 - \frac{\omega_1}{i_m\omega_{t,N}a_{\text{opt}}} \tag{8}$$

where i_m is the gear ratio of the main gearbox, $\omega_{t,N}$ is the rated speed of the turbine, and ω_1 is the synchronous speed of the

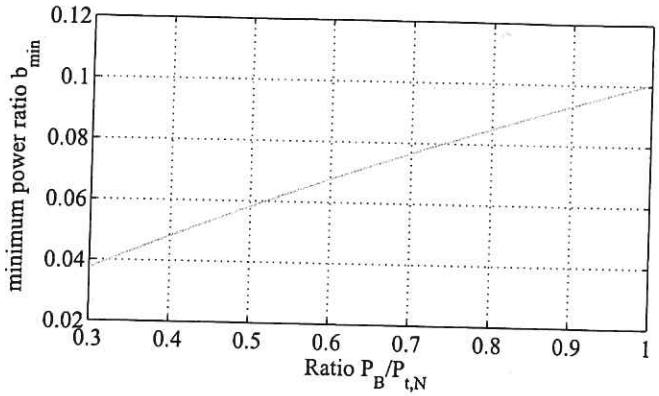

Fig. 4. Minimum power ratio delivered to the servo PMSM.

SG in mechanical radian. The ideal minimum power ratio of the servo PMSM is shown in Fig. 4. Therefore, for the structure in Fig. 1, the ideal minimum power split can be less than 10% of the rated power of the turbine, which indicates the possibility for the reduction of power electronic devices.

III. Control of the Wind Turbine

Since the structure of the wind turbine with power split is more complicated when compared to the existing standard wind turbines, particular attention has to be paid to the control of the drive train of the wind turbine with power split. The control scheme of the wind turbine with power split can be divided into five parts: pitch control, active and reactive power control, the synchronization of the SG, and the control of the back-to-back converter. The control diagram and the signal flow of the proposed wind turbine are shown in Fig. 5. In the figure, T, ω, u, and i denote the torque, rotational speed, voltage, and current, respectively. The subscripts t, sh, and syn denote the turbine, main shaft, and SG, respectively. The superscript $*$ represents the reference value. β is the pitch angle and I_F is the excitation current of the SG. S_{abc} is the switching signal for the rotor-side converter. For the grid-side control of the back-to-back converter, existing strategies such as reported in [19] for the traditional wind turbines can be applied. For the reactive control of the wind turbine, it can be easily achieved by the standard exciter control and automatic voltage regulator (AVR) in the electrical excited SG. Therefore, the reactive power of the wind turbine with power split can be regulated in the same way as the conventional hydropower plant, which is more convenient than that in the existing WT-DFIG and WT-SG. For the pitch control, synchronization and active power control, they have to be designed on the basis of the structure of the planetary gearbox [12].

A. Synchronization of Synchronous Generator

In the wind turbine with a planetary gearbox, the SG is directly connected to the power grid. The synchronization for the SG has to be fulfilled during the transient operation of the wind turbine. Fortunately, the SG itself is a stable system during the transient operation such as sudden load change. It can recover synchronism when the mechanical power does not exce maximum pull-down power [20]. The extracted wind pow limited by the pitch control and active power control. More the frequency oscillation is damped by the damper windi the SG. Therefore, when the SG is properly chosen, no parti attention has to be paid on the synchronization.

B. Active Power Control

The active power control is realized by the servo PMS the wind turbine with power split. Due to the excellent trollability of the servo PMSM, the torque response time reach several milliseconds using both direct torque control field oriented control. This can provide fast torque dynamic protect the wind turbine during wind gust. Since the struc of the planetary gearbox is complicated, it is inconvenien obtain the optimum torque reference for the servo PMSM sidering the losses. The variable speed operation as well as MTTP is realized by the speed control over the speed of main shaft to achieve the optimum TSR. The reference spee the turbine $\omega_t^*(v_w)$ is set to

$$\omega_t^*(v_w) = \begin{cases} \frac{v_w \lambda^*(v_w)}{R_t}, & \text{if } \frac{v_w \lambda^*(v_w)}{R_t} \le \omega_{t,N} \\ \omega_{t,N}, & \text{otherwise.} \end{cases}$$

Here, $\lambda^*(v_w)$ is the optimum TSR according to the wind spe The reference speed for the main shaft is obtained by

$$\omega_{sh}^*(v_w) = i_m \omega_t^*(v_w). \quad ($$

Using (2), the dynamic of the speed on the main shaft ω_{sh} be formulated as follows:

$$\dot{\omega}_{sh} = -k_{11}\omega_{sh} - k_{12}\omega_{syn} + a_{11}T_{sh} + a_{12}T_{syn} + i_z a_{13} T_{servo} \quad (3$$

where T is the torque and the subscripts sh, syn, and ser denote the main shaft, SG, and servo PMSM, respectively. is the gear ratio of the additional transmission gearbox. For t convenience of the controller design, (11) is reformulated int

$$\dot{\omega}_{sh} = -k_{11}^*\omega_{sh} + i_m a_{13}^* T_{servo} + T_{dis} \quad (1$$

where k_{11}^* and a_{13}^* are the references for the coefficients k_{11} a a_{13}. T_{dis} is a general disturbance represented by

$$T_{dis} = -(k_{11} - k_{11}^*)\omega_{sh} - k_{12}\omega_{syn} + a_{11}T_{sh} + a_{12}T_{syn} + i_z(a_{13} - a_{13}^*)T_{servo}. \quad (1$$

Since it is costly to measure or estimate the disturbance torq T_{dis}, a sliding mode controller over the speed of the main sha is introduced to improve the performance. Denoting T_{dis}^{max} the bound of the disturbance, we have $|T_{dis}| < T_{dis}^{max}$. A slidir plane is chosen as

$$s = \omega_{sh}^* - \omega_{sh} + c\int(\omega_{sh}^* - \omega_{sh})dt \quad (1$$

where c is a positive constant. Considering the Lyapunov fun tion $V = \frac{s^2}{2}$, its derivative is shown as follows:

$$\dot{V} = s[k_{11}^*\omega_{sh} - i_z a_{13}^* T_{servo} - T_{dis} + c(\omega_{sh}^* - \omega_{sh})]. \quad (1$$

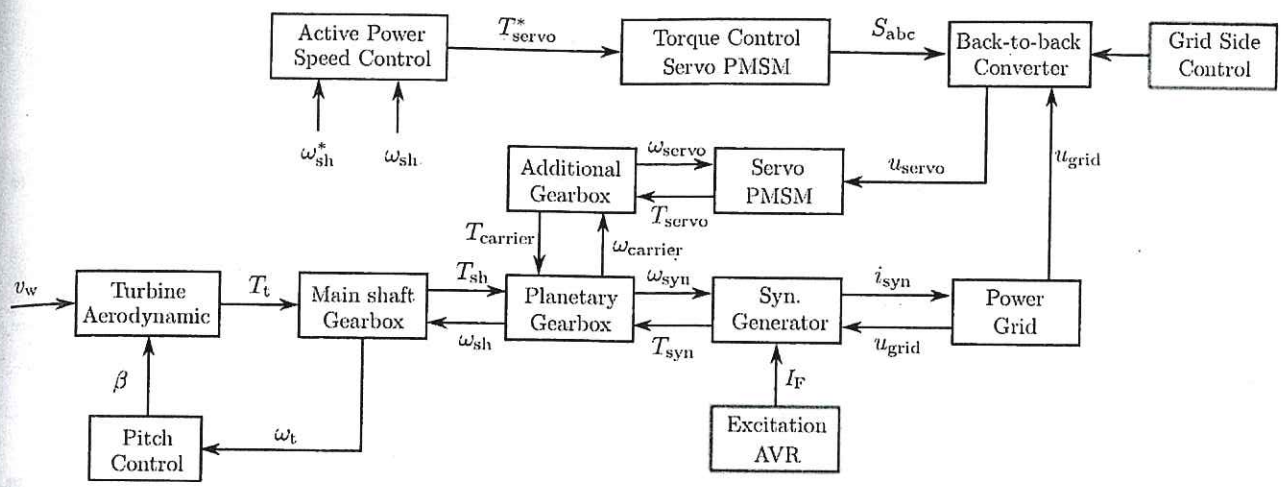

Fig. 5. Control diagram and signal flow for the proposed wind turbine.

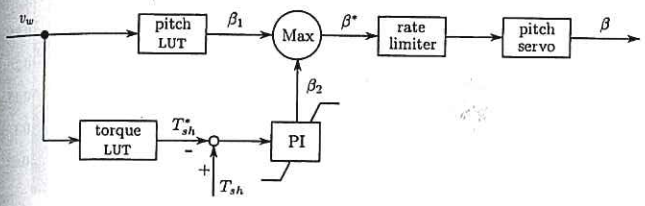

Fig. 6. Pitch control of the wind turbine with power split.

Using the standard design of sliding mode controller

$$T_{\text{servo}} = \frac{1}{i_z a^*_{13}}[\text{sign}(s)T^{\max}_{\text{dis}} + k^*_{11}\omega_{\text{sh}} + c(\omega^*_{\text{sh}} - \omega_{\text{sh}})] \quad (16)$$

the derivative of the Lyapunov function is reformulated into

$$\dot{V} = s(-T_{\text{dis}} - \text{sign}(s)T^{\max}_{\text{dis}}) \leq 0. \quad (17)$$

The equal holds if and only if $s = 0$. Therefore, the sliding mode controller (16) ensures that the optimum TSR of the turbine as well as the MTTP can be achieved. In order to eliminate the chattering effect for the sliding mode controller, the discrete function $\text{sign}(s)$ is replaced by its continuous approximation

$$f(s) = \begin{cases} \frac{s}{\sigma}, & \text{if } |s| < \sigma \\ \text{sign}(s), & \text{otherwise} \end{cases} \quad (18)$$

where σ is a small positive constant.

C. Pitch Control

Since the active power control is realized by the speed control of the main shaft, the pitch angle may be stabilized to the nonoptimal value, when a pitch controller on turbine speed is applied. It is possible that the extracted wind power is much smaller than the optimum value at high wind speed [12]. Therefore, a pitch controller over the torque of the main shaft is implemented.

The structure of the pitch controller is shown in Fig. 6. It contains the look-up table (LUT) of the reference pitch angle β_1, which is the solution of the following equation at different wind speed:

$$C_p(\lambda^*(v_w), \beta) = C^*_p(v_w) = \frac{P^*_t(v_w)}{0.5\rho_{\text{air}}\pi R^2_t v^3_w}. \quad (19)$$

Here, $P^*_t(v_w)$ is the reference power of the turbine according to the reference power curve. C^*_p is the reference performance coefficient. The torque LUT $T^*_{\text{sh}}(v_w)$ is also calculated by the power curve of the turbine

$$T^*_{\text{sh}}(v_w) = \frac{P^*_t(v_w)}{\omega^*_{\text{sh}}(v_w)}. \quad (20)$$

A PI controller with an antiwindup is implemented on the torque error to obtain β_2. The rate limiter of the pitch angle depends on the dynamics of the pitch motor. It is usually around $8°\ \text{s}^{-1}$–$10°\ \text{s}^{-1}$ [21].

The pitch controller combining a pitch LUT and a torque control is to guarantee the safety and performance of the wind turbine for both smooth wind speed and wind gust. For smooth wind speed, the pitch LUT is dominant so that the pitch angle is controlled to its optimum value for the optimum wind power capture. During the wind gust, particularly at high wind speed, the sudden increment of the captured wind power results in high torque and unexpected acceleration of the turbine speed. In this case, the torque control is dominant in the pitch controller. When the PI controller is well parameterized with fast dynamics, the torque of the turbine can be controlled within the predefined range by the pitch angle. Therefore, the servo PMSM can provide sufficient torque to counteract the acceleration of the turbine and to protect the wind turbine.

D. Controllability Considering Grid Codes

For the wind turbine with power split, the main SG is electrically excited and directly connected to the power grid. Therefore, it inherits the controllability and advantages of a traditional hydropower plant when considering the grid codes. For the frequency deviation, a droop control is added to the pitch angle to regulate the output active power. Moreover, the demanded

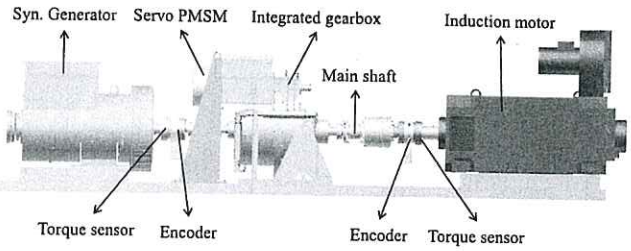

Fig. 7. Structure of the mechanical setup in the test bench.

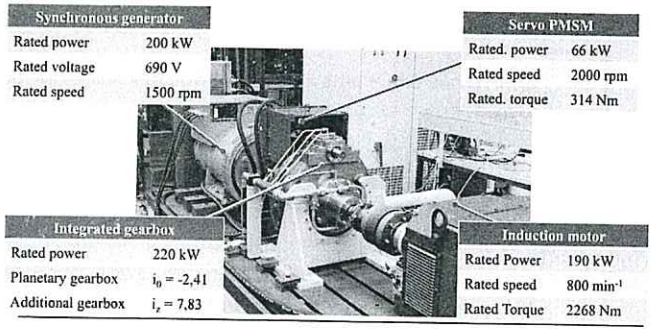

Fig. 8. Data of the experimental setup.

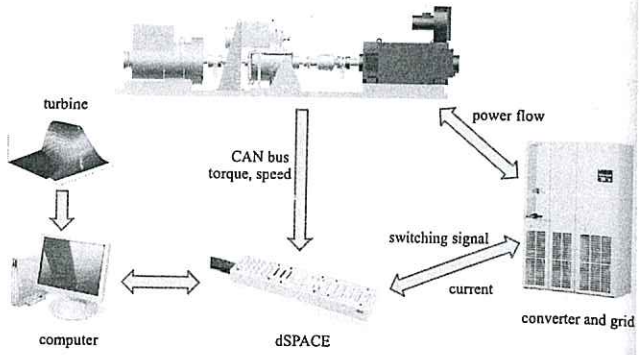

Fig. 9. Structure of the entire system in the test bench.

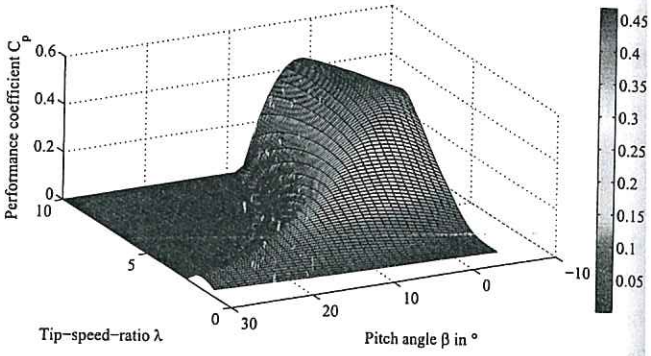

Fig. 10. Performance coefficient of a 6-MW turbine.

voltage and reactive power for the grid codes is easily achieved by the exciter control and AVR system of the SG.

On the other hand, traditional SG has strong fault ride through capability during the system fault such as voltage dip [22]. The exciter control and AVR system of the SG is able to reduce the excitation current to limit the short-circuit current in the generator. Meanwhile, the servo PMSM is disconnected from the converter and can be connected to a crow-bar. In this case, the short-circuit current in the servo PMSM can be damped by the crow-bar and the speed of the servo PMSM is reduced toward 0. Therefore, the wind turbine with power split is able to stay connected with the power grid during voltage dip. Moreover, when compared to the WT-DFIG, the exciter control and AVR system can achieve full controllability of the short-circuit current in the generator. This indicates, the wind turbine with mechanical power split has better fault ride through capability when compared to the WT-DFIG.

IV. Experimental Setup

In order to validate the feasibility, power split behavior and performance of the aforementioned wind turbine with power split, a test bench is constructed (see Fig. 1). The structure of the mechanical system in the test bench is shown in Fig. 7. The induction motor is to emulate the turbine, main gearbox, and the pitch controller. The integrated gearbox is a compact combination of the special planetary gearbox and the additional transmission gearbox. The connection of the special planetary gearbox is shown at the end of Section II-B. The torque and speed of the main shaft, the SG, and the servo PMSM are measured. The ratings of the experimental setup are shown in Fig. 8. The SG is directly connected to the 690-V power grid. The servo PMSM is connected to a back-to-back converter with dc-link voltage 600 V.

The setup for the entire system of the test bench is illustrated in Fig. 9. The experiments are realized by the dSPACE rapid prototyping system with hardware-in-the-loop. The electrical quantities on grid side for the SG and the converter is measured by the Yokogawa power analyzer. For the emulation of the turbine system, the aerodynamics of the turbine, the gear ratio of the main gearbox i_m, and the pitch controller, which are described in the previous sections, are modeled and implemented in the dSPACE system. The emulated torque of the turbine after the main gearbox is realized by the induction motor.

In the test bench, the emulated turbine is down scaled from a 6-MW turbine, whose performance coefficient is shown in Fig. 10. Due to the limited torque of the induction motor, a turbine system with a rated mechanical power of 110 kW is emulated for the experiments. The parameters of the emulated turbine can be found in the Appendix. The power curves shown in Fig. 2 with power ratio $\frac{P_B}{P_{t,N}} = 0.488$ are supplied to the emulated turbine. According to Section II-C, the ideal minimum power split to the servo machine is 5.8% of the rated mechanical of the turbine, while the optimum gear ratio of the main gearbox $i_{m,\mathrm{opt}} = 32.8$. However, due to the very weak field weakening capability of the used servo PMSM and in order to achieve a wide wind speed operation, the gear ratio of the main gearbox i_m deviates from its ideal optimum value.

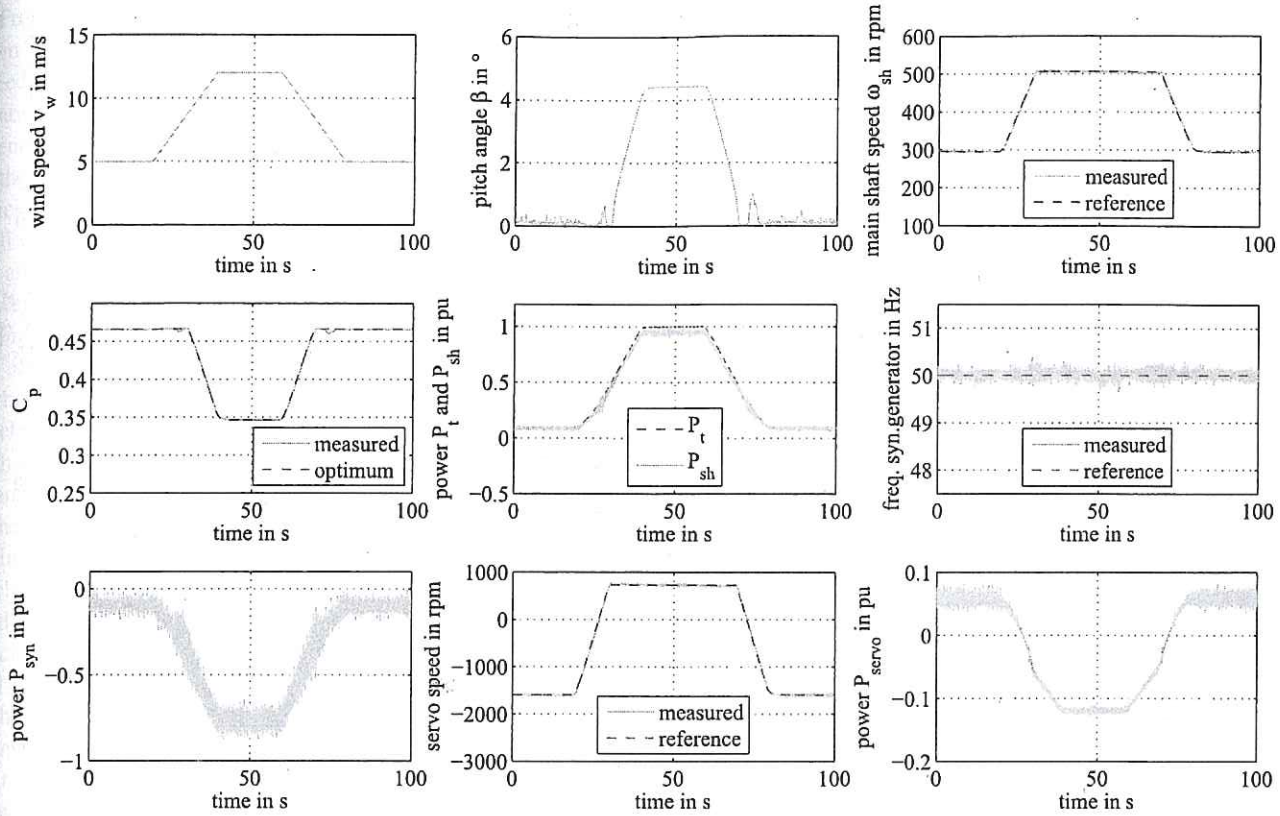

Fig. 11. Experimental results of the wind turbine with a ramp wind speed.

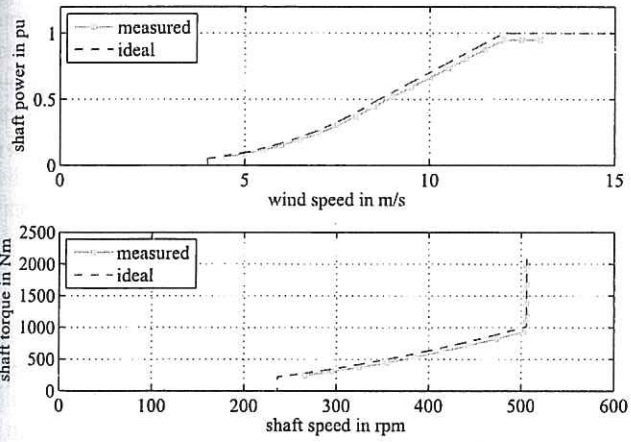

Fig. 12. Ideal and measured operating curves of main shaft.

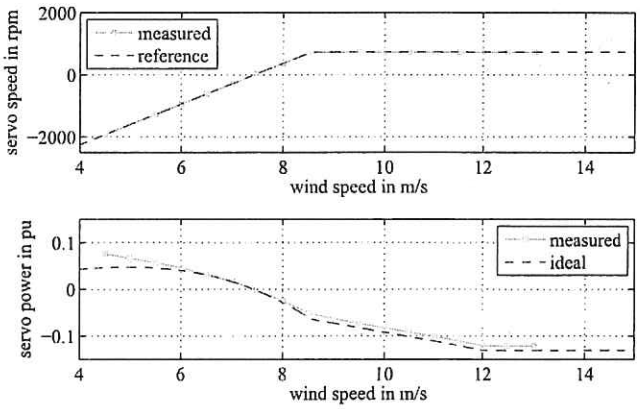

Fig. 13. Ideal and measured operating curves of servo PMSM.

V. Experimental Results

The experiments are performed with ramp, steady state, and stochastic wind to illustrate the performance of the wind turbine with power split. In the experimental results, the positive and negative power represent motor mode and generator mode, respectively. The power is normalized by the rated power of 110 kW.

The experimental results for the ramp wind speed from 5–12 m/s are shown in Fig. 11. The power in the figure is the mechanical power of each component. With the proposed control scheme, the speed of the main shaft closely tracks its optimum reference value so that the optimum TSR is achieved. Moreover, the pitch angle at low and median wind speed is approximately zero, while it increases at high wind speed. The performance coefficient C_p tracks its optimum reference value so that the MPPT can be achieved for the wind turbine with power split. The measured mechanical power P_{sh} delivered to the main shaft is slightly smaller than that of the turbine P_t due to the friction losses. The frequency of the SG stays closely around the grid frequency of 50 Hz so that the synchronization is achieved. The servo machine is used in both motor and

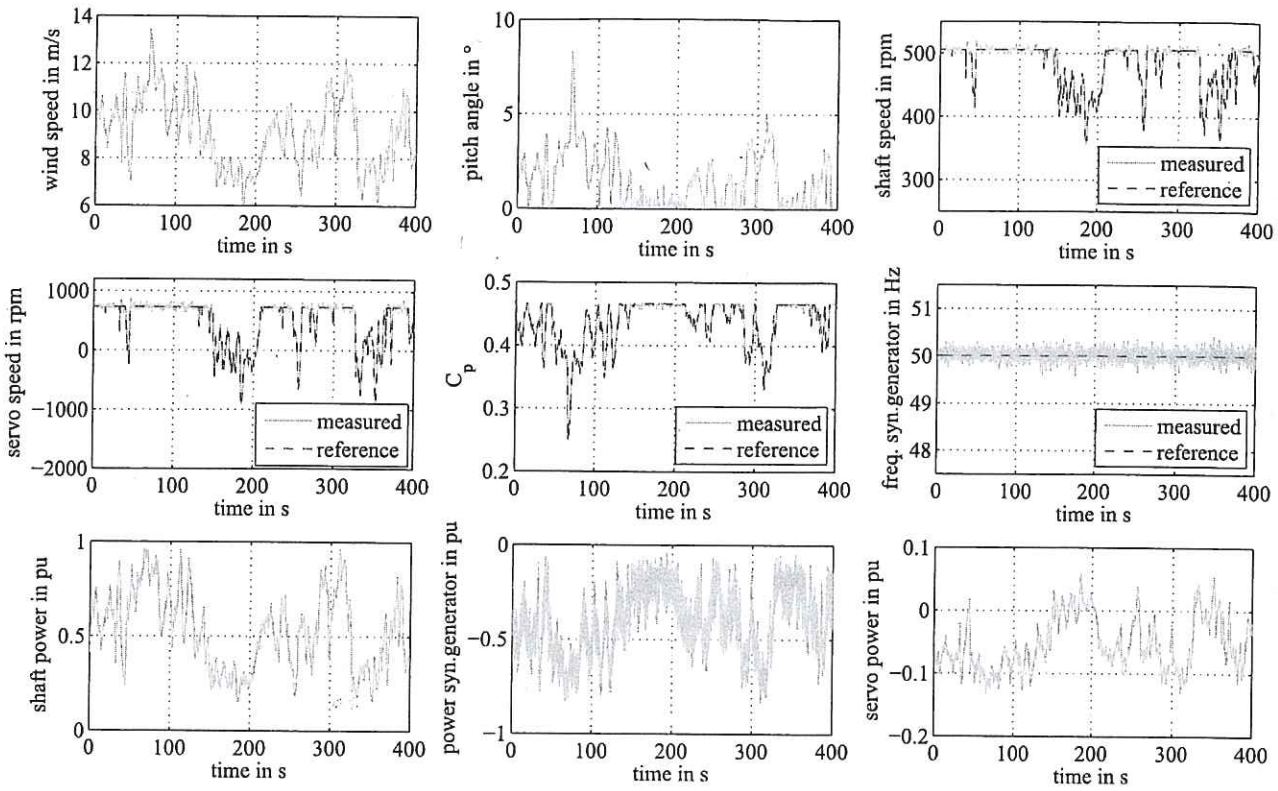

Fig. 14. Experimental results of the wind turbine with stochastic wind speed.

generator operations according to the wind speed. During the variation of the wind speed, the peak mechanical power delivered to the servo PMSM is 0.12 p.u..

In order to illustrate the operating curve of the wind turbine with power split, experiments are made at constant wind speed from 4.5–13 m/s. The operating power and torque curves of the main shaft are shown in Fig. 12. The ideal curve is the power from the wind turbine without friction losses. Therefore, the measured power and torque on the main shaft are slightly smaller than their ideal values.

The operating curves of the speed and power for the servo PMSM are shown in Fig. 13. The ideal curves in the figure are calculated by the model of the planetary gearbox (3)–(6) without friction losses. As shown in Fig. 13, the speed of the servo PMSM matches its ideal value at different wind speed. The measured power curve deviates slightly from the ideal one due to the losses. When the wind speed is low, the servo PMSM is operated in motor mode and it delivers mechanical power to the planetary gearbox. Therefore, the measured power is larger than its ideal value. While the wind speed is increasing, the servo PMSM is operated in generator mode and it is actuated by the planetary gearbox. In this case, the measured mechanical power is smaller than the ideal value. Since the components in the test bench are oversized with almost doubled rated power of the turbine, the operation of each component is in low-efficiency region, particularly at low wind speed. Therefore, the deviation between the ideal and real operating curves of the servo PMSM can be reduced, when the rating of each component is correctly chosen.

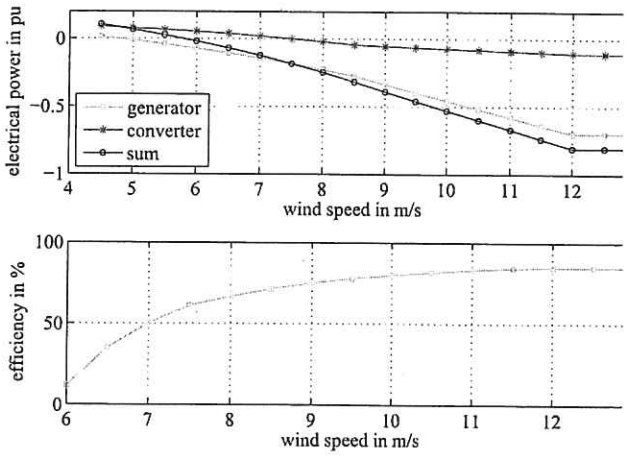

Fig. 15. Measured electrical power and efficiency.

With the nonoptimum gear ratio of the main gearbox, mechanical power of the servo PMSM is within 12% of the ra power of the turbine. This indicates a small power ratio of servo PMSM and its converter, when the PMSM is well desig on the basis of the operating curves. Meanwhile, the electri power of the converter shown in Fig. 15 is within 10.7% of rated power of the turbine, which validates the small power rat Moreover, when the gear ratios of the gearboxes are toward optimum condition (8), the power ratio can approach its id optimum 5.8%.

From Fig. 15, it is shown that the sum of the electrical power from the converter and the SG is larger than 0, when the wind speed is smaller than 5.5 m/s. This indicates that the wind turbine is absorbing power from the power grid. The reason for this phenomenon is due to the overdimension of each component in the test bench, which results in the operation in a very low efficiency region. When the components of the wind turbine are well dimensioned with the appropriate rated power, the losses are able to be greatly reduced and the wind turbine will generate power to the power grid at low wind speed. The efficiency shown in Fig. 15 is the total efficiency of the planetary gearbox and the electrical system. It is calculated by $\eta = \frac{P_{\text{sum}}}{P_{\text{sh}}}$, where P_{sum} is the total electrical power to the power grid and P_{sh} is the mechanical power of the main shaft. The efficiency increases with the augment of the wind speed and reaches 85% at the rated operating point. As mentioned in the previous section, the SG, planetary gearbox, and servo machine in the test bench are not optimized and are twice overdimensioned for the experiments. Each component in the test bench is working in a very low load region, which has a very low efficiency. Therefore, the efficiency of the wind turbine with mechanical power split can still be greatly improved from 85%, when the rated power of each component is correctly designed.

In order to show the feasibility of the wind speed with power split in a realistic situation, the experimental results for stochastic wind speed with wind gust are shown in Fig. 14. The speeds of the main shaft and servo PMSM track their reference values closely. Moreover, the performance coefficient C_p follows its optimum reference value, which is determined by the power curve of the turbine. In the high wind speed region, the main shaft is kept at its rated speed by the pitch controller. The frequency of the SG oscillates around 50 Hz at wind gust and sudden wind speed drop. The major part of the mechanical power is delivered to the SG during the transient operation. The power delivered to the servo PMSM is within 0.12 p.u. with stochastic wind.

VI. Conclusion

In this paper, the structure, power split behavior, and control strategy of a novel concept wind turbine with mechanical power split were introduced and validated by the experiments. The SG in the wind turbine was directly connected to the power grid and the reactive power could be easily controlled by its excitation system. With the control of the servo PMSM and the pitch control, the optimum TSR and MPPT for the wind turbine were achieved. Both theoretically and experimental results showed the small power ratio of the back-to-back converter of the wind turbine with power split. This shows the possibility to reduce the power electronic devices in wind turbines. The feasibility and transient performance of the wind turbine were validated by the experimental results for ramp and stochastic wind speed. Since the wind turbine with power split is with a small-scale converter and without a DFIG, it overcomes the difficulties in WT-DFIG and WT-SG with large power class. Therefore, the wind turbine with power split can be considered as a potential candidate for large-scale wind turbines.

Appendix

TABLE I
Mechanical Parameters of the Test Bench

Rated turbine power	$P_{t,N}$	110 kW
Rated turbine speed	$\omega_{t,N}$	14.19 r/min
Cut-in wind speed	$v_{w,\text{in}}$	4 m/s
Rated wind speed	$v_{w,N}$	12 m/s
Cutoff wind speed	$v_{w,\text{off}}$	20 m/s
Radius turbine rotor	R_t	9.78 m
Gear ratio main gearbox	i_m	35.64
Gear ratio plus planetary	i_0	−2.41
Gear ratio transmission gearbox	i_z	7.83

References

[1] F. Blaabjerg and K. Ma, "Future on power electronics for wind turbine systems," *IEEE Trans. Emerg. Sel. Topics Power Electron.*, vol. 1, no. 3, pp. 139–152, Sep. 2013.

[2] H. A. Mohammadpour and E. Santi, "Modeling and control of gate-controlled series capacitor interfaced with a DFIG-based wind farm," *IEEE Trans. Ind. Electron.*, vol. 62, no. 2, pp. 1022–1033, Feb. 2015.

[3] D. Zhou, F. Blaabjerg, M. Lau, and M. Tønnes, "Optimized reactive power flow of DFIG power converters for better reliability performance considering grid codes," *IEEE Trans. Ind. Electron.*, vol. 62, no. 3, pp. 1552–1562, Mar. 2015.

[4] F. Fateh, W. N. White, and D. Gruenbacher, "A maximum power tracking technique for grid-connected DFIG-based wind turbines," *IEEE Trans. Emerg. Sel. Topics Power Electron.*, vol. 3, no. 4, pp. 957–966, Dec. 2015.

[5] V. D. Colli, F. Marignetti, and C. Attaianese, "Analytical and multiphysics approach to the optimal design of a 10-MW DFIG for direct-drive wind turbines," *IEEE Trans. Ind. Electron.*, vol. 59, no. 7, pp. 2791–2799, Jul. 2012.

[6] H. Li and Z. Chen, "Overview of different wind generator systems and their comparisons," *IET Renew. Power Gener.*, vol. 2, no. 2, pp. 123–138, Jun. 2008.

[7] D. Zhou, F. Blaabjerg, T. Franke, M. Tønnes, and M. Lau, "Comparison of wind power converter reliability with low-speed and medium-speed permanent-magnet synchronous generators," *IEEE Trans. Ind. Electron.*, vol. 62, no. 10, pp. 6575–6584, Oct. 2015.

[8] J. Carroll, A. McDonald, and D. McMillan, "Reliability comparison of wind turbines with DFIG and PMG drive trains," *IEEE Trans. Energy Convers.*, vol. 30, no. 2, pp. 663–670, Jun. 2015.

[9] "xdfm 500-6000," Ingeteam, Milwaukee, WI, USA, 2016. [Online]. Available: www.ingeteam.com/mx/en-us/energy/wind-power-energy/p15_23_253_22/xdfm-500-6000.aspx

[10] X. Rui, L. Li, and X. Li, "Fundamentals of a power splitting driving chain for large wind turbines," in *Proc. 7th World Congr. Intell. Control Autom.*, Jun. 2008, pp. 9347–9350.

[11] Q. Liu, R. Appunn, and K. Hameyer, "A study of a novel wind turbine concept with power split gearbox," in *Proc. 2013 Int. Conf. Electr. Mach. Syst.*, Oct. 2013, pp. 218–222.

[12] Q. Liu, R. Appunn, K. Hameyer, C. Ridder, and E. A. Werner, "Structure and control strategy of a new wind turbine concept with power split," in *Proc. 2nd Conf. Wind Power Drives*, Mar. 2015, pp. 515–528.

[13] T. Ackermann, *Wind Power in Power Systems*, T. Ackermann, Ed. New York, NY, USA: Wiley, 2005.

[14] E. Muljadi and C. Butterfield, "Pitch-controlled variable-speed wind turbine generation," *IEEE Trans. Ind. Appl.*, vol. 37, no. 1, pp. 240–246, Jan./Feb. 2001.

[15] H. Lee and Y. Choi, "A new actuator system using dual-motors and a planetary gear," *IEEE/ASME Trans. Mechatronics*, vol. 17, no. 1, pp. 192–197, Feb. 2012.

[16] J. Zhang, J. S. Dhupia, and C. J. Gajanayak, "Stator current analysis from electrical machines using resonance residual technique to detect faults in planetary gearboxes," *IEEE Trans. Ind. Electron.*, vol. 62, no. 9, pp. 5709–5721, Sep. 2015.

[17] S. Seetharaman, A. Kahraman, M. Moorhead, and Petry-Johnson, "Oil churning power losses of a gear pair: Experiments and model validation," *J. Tribol.*, vol. 131, pp. 022202-1–022202-10, Feb. 2009.

[18] G. Sieros, P. Chaviaropoulos, J. Sørensen, B. Bulder, and P. Jamieson, "Upscaling wind turbines: Theoretical and practical aspects and their impact on the cost of energy," *Wind Energy*, vol. 15, pp. 3–17, Jan. 2012.
[19] A. Merabet, K. T. Ahmed, H. Ibrahim, and R. Beguenane, "Implementation of sliding mode control system for generator and grid sides control of wind energy conversion system," *IEEE Trans. Sustain. Energy*, vol. 7, no. 3, pp. 1327–1335, Jul. 2016.
[20] J. Machowski, J. Bialek, and J. Bumby, *Power System Dynamics: Stability and Control*. New York, NY, USA: Wiley, 2011.
[21] M. Cirrincione, M. Pucci, and G. Vitale, "Neural MPPT of variable-pitch wind generators with induction machines in a wide wind speed range," *IEEE Trans. Ind. Appl.*, vol. 49, no. 2, pp. 942–953, Mar./Apr. 2013.
[22] G. Jenkins and V. Hamidi, "Assessment of fault ride through requirement for distributed generators," in *Proc. 3rd Renewable Power Gener. Conf.*, Sep. 2014, pp. 1–4.

Qian Liu received the Bachelor's degree in electrical engineering from Shanghai Jiao Tong University, Shanghai, China, and the M.Sc. degree in control engineering from the Technical University of Kaiserslautern, Kaiserslautern, Germany, in 2008 and 2011, respectively.

He is currently a Research Associate in the Institute of Electrical Machines, Rheinisch-Westfälische Technische Hochschule Aachen, Aachen, Germany. His current research focuses on high-performance PMSM drive systems and power electronics in electrical vehicles and wind turbines.

Rüdiger Appunn received the M.Sc. and Ph.D degrees in electrical engineering from the Rheinisch-Westfälische Technische Hochschule Aachen, Aachen, Germany, in 2008 and 2015, respectively.

From 2008 to 2015, he was a Research Associate, a Group Leader, and a Chief Engineer in the Institute of Electrical Machines, Rheinisch-Westfälische Technische Hochschule Aachen. Since 2015, he has been with ThyssenKrupp Transrapid GmbH, Munich, Germany. His research interests include magnetic levitation, mechatronics, and inductive power transmission.

Kay Hameyer (M'96–SM'99) received the M.Sc. degree in electrical engineering from the University of Hanover, Hanover, Germany, and the Ph.D. degree in the area of permanent-magnet excited machines from the University of Technology Berlin, Berlin, Germany, in 1986 and 1992, respectively.

After his university studies, he was with Robert Bosch GmbH, Stuttgart, Germany, as a Design Engineer for permanent-magnet servo motors. From 1988 to 1993, he was a Member of Staff at the University of Technology Berlin. From 1996 to 2004, he was a Full Professor of numerical field computations and electrical machines at the Katholieke Universiteit Leuven, Leuven, Belgium. Since 2004, he has been a Full Professor and the Director of the Institute of Electrical Machines, Rheinisch-Westfälische Technische Hochschule Aachen, Aachen, Germany. He has authored/coauthored more than 250 journal publications, more than 500 international conference publications, and four books. His research interests include the design, control, and manufacturing of electrical machines and the associated numerical simulation, in particular, permanent-magnet excited machines and induction machines, and the characterization and modeling of hard- and soft-magnetic materials, numerical field computation, and optimization.

Prof. Hameyer has been a member of the German VDE since 2004 and, since 2002, a Fellow of the Institution of Engineering and Technology, U.K.